Neuronal dynamics underlying communication signals in a weakly electric fish: implications for connectivity in a pacemaker network

Kathleen M Lucas[1], Julie Warrington[1], Timothy J Lewis[2], John E Lewis [1,3]

[1] Department of Biology, University of Ottawa, Ottawa, Canada K1N 6N5

[2] Department of Mathematics, University of California Davis, Davis CA, USA 95616

[3] University of Ottawa Brain and Mind Research Institute, Ottawa, Canada K1N 6N5

Corresponding Author: John Lewis (john.lewis@uottawa.ca)

Highlights

- An electrically-coupled pacemaker network in electric fish sets the timing for its high-frequency electric organ discharge
- Synaptic inputs modulate the timing of this pacemaker on millisecond timescales to produce electrocommunication signals
- These synaptic inputs cause variable resetting of pacemaker neurons resulting in transient desynchronization at the network level
- Computational models illustrate how network connectivity can influence the temporal features of pacemaker resetting
- Differences in pacemaker network connectivity may underlie diversity in communication signals across species

Abstract

Neuronal networks can produce stable oscillations and synchrony that are under tight control yet flexible enough to rapidly switch between dynamical states. The pacemaker nucleus in the weakly electric fish comprises a network of electrically-coupled neurons that fire synchronously at high-frequency. This activity sets the timing for an oscillating electric organ discharge with the smallest cycle-to-cycle variability of all known biological oscillators. Despite this high temporal precision, pacemaker activity is behaviorally-modulated on millisecond time-scales for the generation of electrocommunication signals. The network mechanisms that allow for this combination of stability and flexibility are not well understood. In this study, we use an *in vitro* pacemaker preparation from *Apteronotus leptorhynchus* to characterize the neural responses elicited by the synaptic inputs underlying electrocommunication. These responses involve a variable increase in firing frequency and a prominent desynchronization of neurons that recovers within 5 oscillation cycles. Using a previously-developed computational model of the pacemaker network, we show that the frequency changes and rapid resynchronization we observe experimentally require that neurons be interconnected more densely and with higher coupling strengths than suggested by published data. We suggest that the pacemaker network achieves both stability and flexibility by balancing coupling strength with interconnectivity and that variation in these network features may provide a substrate for species-specific evolution of electrocommunication signals.

Keywords

gap junctions, electrical coupling, neuronal oscillator, synchrony, phase resetting, electric organ discharge

Introduction

Oscillations and synchrony are ubiquitous features of brain networks (Buzsáki and Draguhn, 2004; Steriade, 2006; Buzsáki and Wang, 2012), but too little or too much of either can be pathological (Timofeev and Steriade, 2004; Gonzalez-Burgos et al., 2015; Spellman and Gordon, 2015; Colgin, 2016). Moreover, switching between states that involve oscillatory and/or synchronized firing may be critical for information processing and memory formation (Fries, 2009; Wang, 2010; Hanslmayr et al., 2016; Parish et al., 2018). Therefore, neuronal networks must be robust, keeping oscillations and synchrony under tight control, while being sufficiently flexible to rapidly switch between distinct dynamical states (Haider and McCormick, 2009; Palmigiano et al., 2017).

One network that exhibits this combination of robustness and flexibility is found in the pacemaker nucleus of the weakly electric fish, *Apteronotus leptorhynchus*. The pacemaker nucleus comprises a network of synchronized neurons that sets the timing for the high-frequency (600-1200Hz) electric organ discharge (EOD) (Bennett et al., 1967; Elekes and Szabo, 1985; Salazar et al., 2013) that electric fish use to navigate, capture prey, and communicate (Moller, 2005; Krahe and Fortune, 2013; Lewis, 2014). The EOD is one of the most precise of all biological oscillators, with sub-microsecond variation in cycle period: the coefficient of variation (CV=SD/mean) can be as low as 2×10^{-4} (Moortgat et al., 1998, 2000a). Despite this extreme temporal precision, electric fish can rapidly modulate the EOD on millisecond timescales to produce communication signals called *chirps*. Chirps come in a variety of types and vary across species, but the fastest occur over tens of milliseconds and are characterized by varying decreases in EOD amplitude and increases in instantaneous EOD frequency of up to 500 Hz (Fig. 1B,C) (e.g. Zakon et al., 2002; Zupanc et al., 2006; Hupé and Lewis, 2008; Smith et al., 2016).

Moortgat et al (2000a,b) hypothesized that the highly precise timing of the EOD is a result of dense and strong coupling among neurons in the pacemaker network that effectively “average-out” the noise of individual neurons. Their data however did not support this idea, as each neuron was found to be only weakly coupled via gap junctions to fewer than 5% (between 1% and 7%) of other neurons (Moortgat et al.,

2000a). These authors concluded that network precision is more likely due to very precise firing in individual neurons. However, sparse and weak coupling should render the network prone to instability, with long recovery times following a perturbation; such dynamics are inconsistent with the production of brief electrocommunication signals. How the pacemaker maintains a balance between stability and flexibility is unclear.

In *A. leptorhynchus*, the pacemaker nucleus (Pn) is made up of approximately 150 neurons of two main types: the pacemaker (P) cells, which are intrinsic to the Pn; and the relay (R) cells, whose axons project down the spinal cord to innervate electromotor neurons of the electric organ (Fig. 1A) (Ellis and Szabo, 1980; Elekes and Szabo, 1985; Moortgat et al., 2000a; Smith and Zakon, 2000; Zupanc, 2017). A third class of small interneurons, the parvo cells, has also been identified, but their function is not known (Smith et al., 2000). Pacemaker and relay cells fire synchronously, in one-to-one phase-locking with the EOD cycle (Elekes and Szabo, 1985; Dye and Heiligenberg, 1987). A chirp is elicited by AMPA-type glutamatergic inputs from a subdivision of the prepacemaker nucleus (PPn-C) to relay cells specifically (Dye et al., 1989; Juranek and Metzner, 1998; Zakon et al., 2002). Electrical stimulation of these afferents, both *in vivo* (Juranek and Metzner, 1998) and *in vitro* (Dye, 1988) elicits a chirp-like response in Pn neurons that involves transient increases in action potential frequency and decreases in action potential amplitude. These stimuli can also change the timing relationship between neurons (Dye, 1988), resulting in desynchronization of the pacemaker. However, these dynamics have not been characterized in detail. In addition, while it is known that the Pn comprises a densely-packed, apparently random, network of neurons, with large myelinated axons forming gap junctions via club endings on dendrites, proximal segments and axons (Elekes and Szabo 1985; Moortgat et al 2000a), it has not yet been possible to evaluate the overall network structure.

The goals of the present study are to quantify the responses of Pn neurons to chirp-like synaptic stimulation and then use these responses to evaluate how network connectivity influences Pn function. Using an *in vitro* pacemaker preparation, we show that PPn-C stimulation results in small but variable increases in action potential

frequency of Pn neurons. In addition, we find that the relative timing of spikes between pairs of neurons varies extensively over several post-stimulus cycles, confirming that neurons in the Pn desynchronize during a chirp. We were able to reproduce this behaviour in a network model of the Pn (Moortgat et al., 2000b). However, to match the observed frequency changes and post-stimulus recovery dynamics while also allowing for robust oscillations and synchrony, the model neurons are required to be much more densely interconnected than is supported by previous experimental data.

Experimental Procedures

Animals

Adult brown ghost knifefish (*Apteronotus leptorhynchus*) were obtained from commercial fish suppliers then housed in flow-through tanks containing several individuals. Environmental conditions were held constant with a 12/12 hour light/dark dark cycle with temperature at ~27-28°C, and conductivity at ~150-250 µS. All housing and experimental protocols were in accordance with guidelines approved by the Animal Care Committee of the University of Ottawa (BL-229 and BL-1773).

Tissue Preparation

Tissue preparation protocols were similar to those used previously (Dye, 1988; Moortgat et al., 2000a; Smith and Zakon, 2000; Lewis et al., 2007). Fish were anesthetized with Tricane Methanosulfate (0.2%, TMS, Syndel Canada, Nanaimo, BC) and then transferred to a holder, where their gills were continuously perfused with oxygenated water containing the anesthetic. The brain was then quickly removed and transferred to an ice-cold bath of artificial cerebrospinal fluid (ACSF): NaCl (124 mM), $NaHCO_3$ (24 mM), D-glucose (10 mM), KH_2PO_4 (1.25 mM), KCl (2 mM), $MgSO_4$ (2 mM) and $CaCl_2$ (2 mM). While holding the anterior part of the brain with forceps, the meninges and blood vessels overlying the pacemaker nucleus and surrounding tissues were carefully removed with fine forceps. The pacemaker nucleus, visible as an ovoid protrusion on the ventral brainstem, was then cut away with fine scissors (approximately 1 mm rostral, 0.5 mm caudal, and 1 mm dorsal). The tissue was immediately transferred to a brain slice chamber that was continuously perfused with oxygenated room-temperature (~21°C) ACSF.

Electrophysiological studies

Stimulation protocols were similar to those used by Dye (1988). Bipolar stimuli were delivered through silver wire electrodes, placed rostral of the Pn on each side of the brainstem. Stimuli were constant current pulses (100 µs, 50 µA or 500 µA) delivered using a Multichannel systems STG1004 stimulator (Multi Channel Systems, Reutlingen, Germany). Intracellular recordings were performed with borosilicate

glass microelectrodes (60-90 MΩ resistance; P-2000 electrode puller, Sutter Instrument Company, Novato, CA, USA) using an Axoclamp 2B amplifier (Molecular Devices, Sunnyvale, CA, USA). Data acquisition was performed using a National Instruments PCI-6052E data acquisition board (National Instruments, Austin, TX, USA), at a sampling frequency of 10 kHz using custom Matlab scripts (Mathworks, Natick, MA, USA). Single-pulse stimuli were triggered 0.2 seconds into a 1-second recording sweep, with at least 5 seconds between successive stimuli to prevent long-term frequency changes (Oestreich and Zakon, 2002). Glutamate receptor antagonists AP-5 (50 µM) and CNQX (20 µM) were obtained from Tocris (Minneapolis, MN, USA), and bath applied in the same manner as control ACSF.

Data Analysis

The recordings of the Pn cell membrane potential were analyzed using custom Matlab scripts (MathWorks, Natick, MA). To determine the onset times for each oscillatory cycle (i.e. phase zero), zero-crossings were first calculated for the mean-subtracted membrane voltage waveforms; a linear interpolation between the points immediately below and above zero was used to determine the time of cycle onset. For the phase resetting analysis, post-stimulus cycle periods (T1, T2, T3) were normalized by the control pre-stimulus period, T0 (Fig. 2). The phase difference (ϕ) between a simultaneously recorded neuron pair was defined as the time difference between spikes normalized by the cycle period ($\phi=\Delta t/T0$; Fig. 4). The effect of a stimulus on these phase relationships was quantified by the change in phase difference (i.e. the pre-stimulus phase difference subtracted from the post-stimulus phase difference ($\Delta\phi$; Fig. 4C). We discarded a total of 8 trials (across all cells) because either the stimulus artefact made identification of cycle times ambiguous or cells in a pair were not phase-locked over the pre-stimulus cycles. Unless otherwise indicated, statistical comparisons were made using ANOVA on Ranks in R (www.r-project.org). Some of the experimental data has been presented previously in thesis form (Warrington, 2008).

Network Model

We used a modified computational model of the pacemaker network proposed by Moortgat et al. (2000b). The model included 120 pacemaker and 30 relay neurons, both comprising a somatic and axonal compartment. The somatic compartments are modelled as spheres of diameter d_s; the axonal compartments are modelled as cylinders of length l_a and diameter d_a. Membrane potential dynamics are described using a Hodgkin-Huxley formalism with membrane currents (I_{Na}, I_K, and I_L), synaptic current (I_{syn}), bias current (I_{bias}), coupling current due to gap junctions between neurons (I_c), and the current arising from the adjacent compartment of the two-compartment neuron (I_{axial}); parameter values differed for each neuron type and compartment (Table 1):

$$C\frac{\mathrm{dV}}{\mathrm{dt}} = \mathrm{I_{bias}} + \mathrm{I_c} + \mathrm{I_{axial}} - \mathrm{I_{Na}} - \mathrm{I_K} - \mathrm{I_L} - \mathrm{I_{syn}}$$

The ionic currents are given by:

$$\mathrm{I_{Na}} = \mathrm{g_{Na}m^3h(V - E_{Na})}$$

$$\mathrm{I_K} = \mathrm{g_K n^4 (V - E_K)}$$

$$\mathrm{I_L} = \mathrm{g_L (V - E_L)}$$

The dynamics of each gating variable (m, h, n) are given by:

$$\frac{d\mathrm{j}}{dt} = \alpha_\mathrm{j}(1 - \mathrm{j}) - \beta_\mathrm{j}(\mathrm{j}), \quad \text{where j=m, h, or n}$$

and

$$\alpha_\mathrm{m} = -(\mathrm{V} + 40)\left[\exp\left(-\frac{\mathrm{V}+40}{10}\right) - 1\right]^{-1}$$

$$\beta_\mathrm{m} = 40\exp\left(-\frac{\mathrm{V}+65}{18}\right)$$

$$\alpha_\mathrm{h} = 0.7\exp\left(-\frac{\mathrm{V}+65}{20}\right)$$

$$\beta_\mathrm{h} = 10\left[\exp\left(-\frac{\mathrm{V}+35}{10}\right) + 1\right]^{-1}$$

$$\alpha_{\mathrm{n}} = -0.1(\mathrm{V}+55)\left[\exp\left(-\frac{\mathrm{V}+55}{10}\right)-1\right]^{-1}$$

$$\beta_{\mathrm{n}} = 1.25\exp\left(-\frac{\mathrm{V}+65}{80}\right)$$

The somatic and axonal compartments of each neuron are coupled by an axial current $I_{axial} = g_a (V_{adj} - V)$, where g_a is the axial conductance and V_{adj} is the membrane potential of the adjacent compartment.

Model neurons are coupled electrically through gap junctions with a conductance g_c, such that the coupling current to cell 1 from cell 2 is $I_c=g_c(V_2-V_1)$ where V_2 and V_1 are the membrane potentials of the appropriate compartment of each cell. Unless otherwise noted, the gap junction conductance (g_c) for all connections was set to 0.00001 mS (i.e. 10 nS), which is at the top of the range used in the original model by Moortgat et al. (2000b). Connections between pacemaker neurons, from pacemaker-to-relay and from relay-to-pacemaker are axo-somatic (axon compartment to soma compartment) and fully-rectifying ($I_c=0$ if $V_2<V_1$); connections between relay neurons are soma-to-soma and non-rectifying. Random networks were generated based on connectivity parameters that describe the likelihood of one neuron type connecting to another (P:P, pacemaker-to-pacemaker; P:R, pacemaker-to-relay; R:P, relay-to-pacemaker; R:R, relay-to-relay); unless otherwise indicated, P:P=7%, P:R=10%, R:P=6%, and R:R=23%, based roughly on previous experimental data (Dye and Heiligenberg 1987; Dye, 1988; Elekes and Szabo, 1985; Moortgat et al., 2000a), but slightly different from the original model (where P:P=7%, P:R=35%, R:P=0%, R:R=0%) that was optimized based on cycle-to-cycle variation specifically (Moortgat et al., 2000b).

Synaptic stimulation is modelled as an alpha-function conductance (G_{syn}) with equilibrium potential equal to zero ($E_{syn}=0$), delivered to a fraction of the relay neuron population (see Results):

$$\mathrm{I}_{\mathrm{syn}} = \mathrm{G}_{\mathrm{syn}}(\mathrm{V}-\mathrm{E}_{\mathrm{syn}})$$

$$\mathrm{G}_{\mathrm{syn}}(t,t_o) = \mathrm{g}_{\mathrm{syn}}\left(\frac{t-t_o}{\tau}\right)\exp\left(-\frac{t-t_o-\tau}{\tau}\right),\ \ t \geq t_o$$

where g_{syn} determines the strength of the synaptic connection (e.g. g_{syn} = 0.00009 mS, or 90nS) and τ is the time-to-peak (τ = 1.83ms; Dye 1988). Numerical simulations were performed using the Euler method with a time step of 0.5µs. Model parameters are based on Moortgat et al. (2000b) and are shown in Table 1. For this parameter set, isolated pacemaker neurons fire action potentials at 678 Hz, but isolated relay neurons do not fire spontaneously. In our initial analysis, we generated 10 random networks using the connectivity parameters above with the condition that the network recovered to the original synchronous state after stimulation. Phase resetting curves and change in phase ($\Delta\phi$) were calculated for model neurons, as in the experimental analyses. We also explored network responses over a range of connectivity parameters (g_c from 5 nS to 15 nS, and P:P from 2% to 40%). In these studies, we generated either 10 (Fig. 8) or 100 (Fig. 9) unique networks (see Results) for each parameter set (pair of g_c, and P:P values).

Results

In the following, we first describe the responses of neurons in the pacemaker nucleus (Pn) to the synaptic inputs that underlie electrocommunication signalling. In doing so, we experimentally test the hypothesis that the communication signal called a chirp involves the transient desynchronization of Pn neurons. We then use a computational model of the Pn to explore the network features that can account for the experimentally observed responses.

Pacemaker (Pn) network *in vitro*

Using an *in vitro* Pn preparation (Dye 1988), we explored the effects of electrically stimulating synaptic inputs from the PPnC on the timing and phase relationships of Pn neurons. Figure 2A shows an example of a simultaneous recording from a pacemaker (P) and relay (R) neuron. In general, it is possible to identify cell type by membrane potential waveform (Bennett et al., 1967). The action potentials of R neurons do not exhibit a gradually depolarizing rising phase (pacemaker potential), so appear less symmetrical than those of P neurons (Fig. 2A). In this example, the stimulus (500 μA amplitude) produced slight changes in spike timing (<3% of the control cycle period, T0), as well as a decrease in amplitude of the R neuron action potential. In a second example (Fig. 2B), two stimulus trials with the same stimulus timing resulted in different responses in the same P neuron (spike timing and amplitude vary). In the following analyses, we characterize this variability using two temporal features of the responses: (1) changes in the oscillation cycle period (interspike interval) of individual neurons as a function of stimulus timing (phase resetting curve), and (2) changes in the relative timing among pairs of neurons, i.e. change in phase difference ($\Delta\phi$).

Phase resetting curves

We first quantified the changes in Pn cell cycle duration as a function of the stimulus phase. These phase resetting curves included the first three post-stimulus cycles (T1, T2, T3; Fig. 2A) in a total of 40 neurons (29 P neurons, 11 R neurons in 8 fish). A weak 50 μA stimulus had no significant effect on normalized cycle durations (median and [interquartile range] over all cells: T1=1.00 [0.998, 1.005]; T1=2.00 [1.994, 2.005];

T1=3.00 [2.993, 3.007]). In contrast, a stronger 500 μA stimulus produced variable changes in cycle duration with a trend towards shortening at all stimulus phases (Fig. 3A; median and [interquartile range] for P neurons: T1=0.99 [0.975, 1.006; T2=1.95 [1.887, 1.998]; T3=3.00 [2.979, 3.005]; and for R neurons: T1=1.00 [0.984, 1.016]; T2=1.92 [1.877, 1.960]; T3=2.98 [2.953, 3.001]). These effects were weakly (but not significantly) dependent on stimulus phase (p=0.07) and cell type (p=0.08, two-way ANOVA on ranks). Closer inspection of T1 (Fig. 3B) shows that these trends are reflected in the individual cells as well and that some individual neurons had very different responses to similar stimulus phases (filled symbols in Fig. 3B are for an individual cell of each type). In summary, the 500 μA stimulus produced relatively small decreases in cycle duration that were variable across the population of cells as well as a single cell. In the context of a chirp, changes in cycle duration of a similar magnitude would result in a 40-60Hz increase for a fish with an EOD frequency of 800Hz (similar to a type II or small chirp, Fig. 1; Zakon et al 2002; Smith et al 2016). In the next section, we quantify changes in the firing relationship between cells (change in phase difference, $\Delta\phi$) to assess the impact of response variability on the synchrony of neurons in the pacemaker during a chirp stimulus.

Change in phase difference between neuron pairs

Similar to previous studies (Dye 1988; Moortgat et al 2000a), we found that pairs of neurons were in general phase-locked with near non-zero phase differences during on-going pacemaker activity (i.e. not perfectly synchronized with zero-phase difference). Figure 4B shows a histogram of phase difference (defined in Fig. 4A) for the 20 pairs of neurons in our data set. The distribution is consistent with previously reported data (Dye 1988; Moortgat et al 2000a); the largest phase differences (0.13 and 0.19 in Fig 4B) occur between pacemaker and relay (PR) cell pairs and the smallest between P cell pairs. The variable change in cycle duration described in the previous section suggests that these phase relationships change in response to a chirp stimulus. We therefore measured the change in phase difference ($\Delta\phi$) produced by the stimulus (i.e. if the stimulus does not change the relative timing of action potentials between the cell pairs, then $\Delta\phi$ is zero). Because cycle duration does not significantly depend on stimulus phase, we combined data across stimulus

phases for this analysis. As expected, the weak 50 µA stimulus produced little change in ϕ over 10 post-stimulus cycles (absolute value of $\Delta\phi$=0.0027 [0.0012, 0.0058], median and [interquartile range] over N=16 cell pairs). The 500 µA stimulus however (Fig. 4C) caused a significant change in phase difference (ANOVA on ranks, $p \approx 10^{-14}$; N=20 cell pairs) over the first four post-stimulus cycles in a manner that depended on neuron pair type ($p \approx 10^{-5}$); these differences are due largely to an increase in variance over the first four post-stimulus cycles. Overall, this increased variability in phase difference confirms that a chirp stimulus not only increases frequency but also desynchronizes neurons in the pacemaker nucleus.

The *in vitro* Pn preparation contains the projections from two different brain areas, the diencephalic prepacemaker nucleus (PPn) and the mesencephalic sublemniscal prepacemaker nucelus (SPPn). Slow EOD modulations occurring over minutes, are elicited by glutamatergic input from the SPPn and the PPn subdivision PPn-G (PPn-Gradual rise) via NMDA receptors on both P and R neurons (Heiligenberg et al., 1996; Juranek and Metzner, 1997, 1998; Oestreich and Zakon, 2002). Chirps on the other hand are elicited via glutamatergic inputs from the PPn subdivision PPn-C (PPn-Chirping) through activation of AMPA receptors on R cells (Dye et al., 1989; Juranek and Metzner, 1998). We therefore selectively blocked the NMDA-type inputs from PPnG and SPPN, and the AMPA-type inputs from PPnC in 5 cell pairs. The NMDA receptor antagonist AP-5 (50 µM) did not alter the $\Delta\phi$ response; similar to control conditions, stimulation resulted in a significant change in phase over five post-stimulus cycles ($p<0.001$). However, blocking AMPA-type inputs from the PPnC with CNQX (20 µM) eliminated the stimulus-induced change in phase over all post-stimulus cycles ($p=0.45$). This, along with the fact that the brief single-pulse stimuli used here do not elicit NMDA-induced long-term changes in the pacemaker frequency (Oestreich and Zakon, 2002), suggests that the effects we observe are dominated by the chirp-specific AMPA-type synaptic inputs from PPnC.

Pacemaker (Pn) network models

Moortgat et al (2000b) developed a network model to investigate the experimentally observed precision and synchrony of the Pn. Here, we use this model to explore

pacemaker network dynamics in the context of our experiments using synaptic stimulation. In particular, we focus on two parameters that can have a significant impact on network synchronization: (1) the likelihood of connections between neurons (network connectivity), and (2) the strength of these connections (gap junctional conductance, g_c). As described in the Experimental Procedures, we generated random model networks of 120 P and 30 R neurons connected via gap junctions using connectivity probabilities based on previous work (Moortgat et al 2000b): pacemaker-to-pacemaker P:P=7%, pacemaker-to-relay P:R=10%, relay-to-pacemaker, R:P=6%, and relay-to-relay R:R=23%. Note that this connectivity was slightly more dense than estimated from experimental observations (Moortgat et al 2000a; Elekes and Szabo, 1985), but this was necessary to achieve a sufficiently low CV (Moortgat et al 2000b). The gap junctional conductance (g_c) was set to 10 nS, at the top of the range used by Moortgat et al. (2000b). We used an alpha-function synaptic conductance to generate the EPSP produced by the brief stimulus used in our experiments (see Experimental Procedures).

Figure 5 shows representative network responses elicited when a stimulus (g_{syn} = 90nS) was delivered simultaneously to 15 relay (R) cells (half of the R cell population). In all panels, the first four cycles (Fig. 5, pre-stimulus) show the stable near-synchronous firing state; membrane potential traces are overlays of all neurons (120 P and 30 R neurons) so the thickness of the traces are related to the level of synchrony. We found similar responses for different stimulus phases in the same network (compare Fig. 5A and B). The firing rate of R neurons receiving direct input (dark red) was transiently increased (period decreased), whereas the other R neurons (light red) became slightly less synchronized with relatively little change in frequency. There was also a variable decrease in action potential amplitude in the stimulated R neurons, with an occasional skipped or additional spike. The pacemaker (P) neurons responded in a much more consistent manner, with a decreased level of synchrony and only a small change in frequency or action potential amplitude (similar to the unstimulated R neurons). While the stimulus had a greater effect on R neurons during the first cycle, the effect spread to P neurons over subsequent cycles. These observations were similar across different networks with the same

connectivity parameters (compare responses to the same stimulus in three different networks, Fig. 5 A, C and D).

To illustrate the response properties of the model networks in more detail, we show a phase resetting analysis for one example network using a slightly weaker stimulus (g_{syn} = 90nS applied to 10 R neurons). While in general, noise sources in the experiments contribute to more variable responses, the phase resetting curves from model networks are similar to those observed in the experiments. The stimulus caused a small decrease in cycle duration that was variable across individual neurons (Fig. 6A,B). There is some dependence on stimulus phase in the first cycle (T1), especially for R neurons. When the stimulus was applied in the first part of the cycle (stimulus phase of 0 to 0.5), there is a bimodal response in R neurons, with the lower band (phase advance) representing the neurons receiving direct inputs (see Fig. 5, dark red). This propagates through the network, producing increased timing variability for both P and R neurons in subsequent cycles (T2 and T3) that alters the initial dependence on stimulus phase. In the experimental curves, the phase dependence of T1 was seen in later stimulus phases (>0.5); this difference could be due to synaptic or propagation delays that were not included in the model. Small changes in stimulus strength (defined by the value of g_{syn} and the number of R neurons receiving inputs) resulted in qualitatively similar responses, with stronger stimuli producing larger effects on cycle period (Fig. 6C,D show mean responses over all cells of a given type). For the intermediate stimulus used in Fig. 6A,B, the decreases in cycle period were similar to those seen in experiments, with the exception of T1 in R neurons which was about 10% larger (Fig. 6C,D; compare colored lines for "90nS on 10 R cells" to dashed-line showing median responses for T2 in the experiments).

We also measured the change in phase difference ($\Delta\phi$) between cells in the model network (Fig. 7A; combined data from all stimulus phases as in Fig. 4C) produced by the stimulus used for Fig. 6A,B. As in the experiments, the model neuron pairs were transiently desynchronized after the stimulus. The variability in phase difference between model neurons generally increased over the first few post-stimulus cycles, with a peak $\Delta\phi$ for all pair types occurring in the third post-stimulus cycle (Fig. 7A). In

general, recovery was slower than in experiments, with stimulus effects lasting longer than 5 cycles (Fig. 7B). These effects depended on the stimulus: larger values of g_{syn} acting on more R neurons produced larger and longer lasting effects (Fig. 7B). In some cases, the strongest stimuli perturbed the network such that it did not recover to its original synchronized state (see Fig. 7B, light gray in lower panel). Note that while the stimulus used for the responses shown in Fig. 7A (g_{syn}=90nS on 10 relay neurons) produces resetting responses that are similar in magnitude to those observed experimentally, the effects on phase difference are much stronger (Fig. 7B upper panel; compare open symbols with light gray closed symbols). In order to match the recovery of phase differences to those in experiments, a much weaker model stimulus was required (g_{syn} =50nS onto 15 relay cells; Fig. 7B, middle panel). Indeed, the results shown in Figures 6 and 7 suggest that a single stimulus magnitude can not easily account for both the phase resetting and changes in phase differences observed in the experiments. To address this inconsistency, rather than optimizing model parameters to precisely fit the data, we instead explore the influence of different network features using a broad survey of randomly generated networks with varying properties.

Influence of network connectivity on post-stimulus response

Previous modeling of the pacemaker (Pn) network focused on reproducing the high level of firing precision (i.e. low CV of oscillation period) (Moortgat et al 2000b). The results presented in the previous sections suggest that, in addition to oscillator precision, network stability (i.e. ability to recover from a chirp-like synaptic perturbation) should also be considered when evaluating pacemaker network models. Thus far, we have shown that the Pn network model captures at least some features of Pn dynamics. However, for a given stimulus strength, there is a mismatch in the resetting responses and recovery times between experiment and model. Therefore, we further explored network response properties as determined by two parameters that control the strength and density of network connections respectively: gap junctional conductance (g_c) and pacemaker connectivity (P:P).

We generated 10 unique random networks for a given pair of values of P:P connectivity and gap junctional conductance. We characterized the responses of

model P and R neurons to a relatively large synaptic stimulus (g_{syn} =90nS onto 15 R neurons, as in Fig. 6A,B and Fig. 7A) that results in longer recovery times, and thus an increased ability to detect differences between networks. Our analyses focused on three metrics: (1) "chirp FM", the frequency increase as indicated by the minimum cycle duration (averaged over all cells) in the first 5 post-stimulus cycles; (2) "chirp AM", the peak level of desynchronization as indicated by the maximum variation in phase difference between cell pairs (peaks of curves in Fig. 7B); and (3) "chirp duration", the post-stimulus recovery time, as indicated by the number of cycles required for neurons to re-synchronize following a stimulus. We consider these three metrics as analogs to those commonly used to describe chirp responses i.e. chirp frequency modulation (FM), chirp amplitude modulation (AM), and chirp duration, respectively (e.g. Smith et al 2016).

In general, P neuron response metrics decreased with increasing network connectivity, i.e. increases in P:P and g_c (Fig. 8). The largest effects are seen in chirp duration (Fig. 8E, blue), with recovery times becoming more than three times faster as networks become more densely coupled (P:P increases from 4% to 30%; g_c=5nS). The effect of g_c on recovery is largest for P:P less than 10%, with networks recovering about twice as fast when g_c = 15nS compared to g_c = 5nS. For more dense networks, increasing g_c had relatively little effect. Interestingly, the overall effects on R neurons was much less. Again, chirp duration was most sensitive, decreasing slightly with increases in g_c (mean over all networks of 6.2 and 4.6 cycles for g_c = 5 and 15nS respectively; Fig. 8E,F, red) but changing relatively little with changes in P:P connectivity. These results suggest that R neurons are buffered somewhat from chirp-induced changes in P neuron dynamics, at least when coupling strength (g_c) is low. Note however that because the stimulus acts directly on R neurons, the overall effect of the stimulus on R neurons is generally much larger than on P neurons: chirp FM (maximum shortening, Fig. 8A,B), chirp AM (peak phase variation, Fig. 8C,D), and chirp duration (recovery time, Fig. 8E,F) are in general greater for R than P neurons.

Changes in g_c and P:P can have a strong effect on the coefficient of variation of the cycle period (CV) of the model networks (Moortgat et al 2000b). We found that, as

long as P:P was greater than 4%, the CV of P cell activity was at the limit of our numerical precision (~$3x10^{-4}$) and thus very close to the smallest experimentally-observed levels. The CV of R cell activity was similarly low for large values of g_c (15nS), but for g_c= 5nS, increased to $5.1x10^{-3} \pm 4.2x10^{-3}$ (mean±SD over the 10 networks). Compared to that of P cells, the variability in CV for R cells from network-to-network was marked, ranging from values ~10^{-4} to more than 10^{-2}, two orders of magnitude above that seen in experiments (Moortgat et al 1998). Note that this variability is due to the dynamics of the system (i.e. attractors that are not simple limit cycle oscillations) as there are no stochastic noise terms in the model.

Many of the random networks we considered here exhibited asynchronous states and signs of multistability and thus sometimes failed to recover to the original synchronized state after a stimulus perturbation (see Fig. 7B, lower panel). These responses were not included in the results shown in Fig. 8, but such behavior is nonetheless worth considering. The EOD fires continuously, without pause, for the life of the fish so the pacemaker network must be robust to perturbation. How likely is it that the model networks we have described are as robust as the real pacemaker? To answer this question, we generated additional sets of 100 random networks for each set of network parameters (g_c and P:P) and asked what percentage of these networks recovered within 10 post-stimulus cycles (recovery indicated by median $|\Delta\phi|<0.01$). Figure 9 shows that for g_c=5nS, a very small fraction of networks are stable when P:P=4% (the experimental estimate for pacemaker connectivity; Moortgat et al 2000a). This fraction increases with increased gap junctional conductance (g_c=10nS and 15nS) and increased values of P:P, but to achieve a large fraction of stable networks, network connectivity (g_c and P:P) must be stronger and much more dense than previously predicted for the pacemaker network. Interestingly, Moortgat et al (2000b) used P:R connection probabilities much higher than experimental data suggests to achieve the robustness required for their analysis of pacemaker oscillation CV .

Overall, these model networks can show stimulus-response dynamics that are similar to those described in the experiments. Although sufficiently fast post-stimulus resynchronization can be achieved in some weak and sparse networks, this depends

on the details of the connectivity; fewer than 5% of networks generated with g_c=5nS and P:P=4% resynchronized at all. Taking into account responses to chirp-like stimuli, post-stimulus recovery dynamics, and oscillator CV suggests that P:P connectivity should be at least 10-15% with g_c close to 15nS. These values are about double what has been predicted from experimental measurements (Moortgat et al 2000a,b). In addition, our results suggest that chirp parameters will be more readily controlled by the synaptic inputs to relay neurons in sparse, weakly coupled networks. However, in more highly-connected networks, pacemaker cell dynamics along with changes in strength and density of pacemaker connectivity will have a greater effect on the temporal dynamics of chirping.

Discussion

Our study describes a quantitative analysis of the network dynamics of a high-frequency, highly-precise neuronal oscillator in the weakly electric fish. We show that a common electrocommunication signal is associated with a transient desynchronization of this pacemaker network and then use this behavior to better understand the functional role of network connectivity. Our results confirm that high oscillator precision (low CV) can be achieved with sufficient electrical coupling (g_c>5nS) in a sparse network (P:P connectivity of 4%), but to ensure physiological levels of stability and robustness, network connectivity is required to be stronger (larger g_c) and more dense (larger P:P) than predicted from previous experimental observations.

Chirping and pacemaker desynchronization

Chirping behavior and its role in electrocommunication across different species of wave-type weakly electric fish has been addressed in many studies (e.g. Zakon et al., 2002; Zupanc et al., 2006; Hupé and Lewis, 2008; Marsat and Maler, 2010; Smith et al., 2016). However, the network mechanisms underlying chirp generation in the pacemaker nucleus has received relatively little attention. Early studies described the synaptic inputs responsible for chirp generation, along with detailed intracellular recordings from pacemaker and relay neurons (Dye and Heiligenberg, 1987; Kawasaki and Heiligenberg, 1988; Juranek and Metzner, 1997, 1998). Using the *in vitro* preparation we have adopted, Dye (1988) provided evidence that a chirp involves a change in phase relationship between neurons (i.e. desynchronization), as well as a transient increase in frequency. We confirmed these results with a quantitative analysis and also showed that responses to chirp-like stimuli are sufficiently variable to mask dependence on stimulus timing. Taken together, these results support the idea that the diversity of chirp types within a species (Zupanc et al., 2006; Turner et al., 2007; Smith et al., 2016) is not achieved by varying the relative timing of synaptic inputs (Walz et al., 2013), but is more likely the result of differences in the strength and recruitment of synaptic inputs. In addition, chirp diversity across species may also involve differences in pacemaker network

connectivity (Heiligenberg et al., 1996; Juranek and Metzner, 1997). The pacemaker nucleus in *Apteronotus albifrons*, a closely related species to that considered here (*Apteronotus leptorhynchus*), has more than twice the number of relay neurons and about 25% more pacemaker neurons. Interestingly, the Pn in *A leptorhynchus* appears to be more densely interconnected through gap junctions and receives a higher density of descending chemical synaptic inputs than in *A albifrons* (Elekes and Szabo 1985). The much longer chirps with a larger FM component in *A albifrons* (Smith et al 2016) is not consistent with weaker descending inputs, and in light of our results suggests that pacemaker connectivity plays an important role in determining chirp properties (e.g. less dense P:P connectivity leads to longer recovery times, Fig. 8E). A more detailed comparative analyses, both at the anatomical and electrophysiological levels, and involving additional species will be required to test these hypotheses.

The desynchronization of Pn neurons during a chirp is not unexpected. The heterogeneity of coupling in a relatively sparse random network will generally lead to differential effects of synaptic stimulation (Vervaeke et al., 2010). Neurons receiving direct inputs will be affected first, and the effects will then spread through the network to indirectly affect other neurons. The differences in spike timing lead to a dispersion in phase difference followed by a gradual return to pre-stimulus levels of synchrony over several oscillation cycles. This is clearly seen in the Pn network models (Fig. 5), where the stimulated relay neurons (dark red) are initially phase-advanced (fire earlier), while a gradual change in pacemaker neuron timing (i.e. phase) occurs over subsequent cycles. In the types of model networks we have considered, the synchronized state did not always recover after synaptic stimulation, and instead revealed other asynchronous states that are not observed experimentally. The instrinsic properties of individual neurons can significantly influence phase resetting properties and the stability of network synchronization (e.g. Pfeuty et al., 2003; Mancilla et al., 2007; Stiefel et al., 2008; Dodla and Wilson, 2013), so it is possible that our model neurons do not adequately represent the dynamics of real Pn neurons. Future work will focus on experimentally evaluating the influence of specific ion conductances (Smith and Zakon, 2000) and

heterogeneities of synaptic inputs on network stability, with an aim towards improving Pn models.

Network connectivity and pacemaker resynchronization

Our results using the synaptically-driven chirp response to evaluate the coupling strength (g_c) and connectivity (P:P) of model Pn networks suggests that the connections in the Pn are stronger and more dense than previously suggested. It is not surprising that previous experimental measurements may have underestimated Pn connectivity. First of all, it is inherently difficult to accurately determine gap-junctional coupling strength between neurons in an intact electrically-coupled network. This is due in part to uncertainties that arise from unknown electrotonic decay over complex spatial geometries, as well as the unknown resistive loads provided by other coupled neurons. In addition, dye-coupling techniques, such as those used in previous studies of the pacemaker (e.g. Moortgat et al 2000a), can be prone to false-negatives (incomplete diffusion of the dye through branching processes and gap junctions) that would lead to underestimates of connectivity. That said, although our results on resynchronization times suggest a strong and densely-coupled Pn network, this may not be consistent with the network flexibility required for chirping: higher levels of network connectivity would likely require stronger synaptic inputs to a greater number of neurons for chirp production, leading to much higher energy demands (Salazar et al 2013).

There may however be other ways to achieve higher network connectivity while maintaining sufficient flexibility for chirp generation. One possibility is that connectivity is more hetereogeneous in the pacemaker than in our simple model networks. For example, stronger, more dense, coupling between relay neurons alone may provide stability and faster recovery, along with low CV, whereas weaker, more sparse, coupling among pacemaker neurons could facilitate transient desynchronization required for a chirp while also minimizing the destabilizing reverberations that can occur in strongly-coupled sparse networks.

Another consideration is that the pacemaker nucleus is a tightly packed network of relatively large cells firing in near synchrony. The resulting field potentials are

significant (Curti et al., 2006; Quintana et al., 2011b, 2011a, 2014) and could lead to increased electrical interactions, thus effectively increasing network connectivity through field effects or ephaptic coupling (Faber and Korn, 1989; Anastassiou et al., 2011). Further, a large number of other cells likely work to modulate and control the extracellular space (Zupanc, 2017). In this way, the pacemaker network may be optimized such that sparse, relatively weak gap junctional coupling allows the flexibility for rapid, transient chirp generation, with ephaptic coupling providing the stability and robustness (high temporal precision and fast recovery from synaptic perturbation) that are not inherent properties of sparse random networks with gap junctional connections alone. Field effects and ephaptic coupling are well-known, but their significance in neuronal processing is not yet clear (Anastassiou and Koch, 2015). With an easily characterized functional output, the pacemaker network is an attractive model in which to address this question directly.

Conclusion

Identifying the mechanisms that allow neuronal networks to be robust and temporally precise, yet flexible enough to rapidly switch between dynamical states is a necessary step towards understanding a variety of brain functions in health and disease. The pacemaker network in weakly electric fish is a neuronal oscillator with a well-defined function, and temporal precision that is under behavioral control for communication signal generation (Moortgat et al., 1998). This, along with the diversity in oscillator frequencies and signalling properties across species (Turner et al., 2007; Smith et al., 2016), suggests that there may be similar diversity in the Pn connectivity. Our results from *A leptorhynchus* show that synaptic stimuli underlying chirp production cause a transient desynchronization-resynchronization among neurons in the pacemaker network. The resulting dynamics suggest that network interconnectivity may be optimized to maintain a balance of stability and flexibility.

Acknowledgements

This work was supported by an NSERC Discovery Grant to JEL.

Author Contributions

All authors designed the research; JW performed the experiments; JW and JEL analyzed the data; KML, TJL and JEL did the modelling. KML, TJL and JEL wrote the manuscript and all authors approved the final version.

The authors declare no competing financial interests.

References

Anastassiou C, Perin R, Markram H, Koch C (2011) Ephaptic coupling of cortical neurons. Nat Neurosci 14:217–223

Anastassiou CA, Koch C (2015) Ephaptic coupling to endogenous electric field activity: Why bother? Curr Opin Neurobiol 31:95–103

Bennett M V, Pappas GD, Giménez M, Nakajima Y (1967) Physiology and ultrastructure of electrotonic junctions. IV. Medullary electromotor nuclei in gymnotid fish. J Neurophysiol 30:236–300

Buzsáki G, Draguhn A (2004) Neuronal oscillations in cortical networks. Science 304:1926–1929

Buzsáki G, Wang X-J (2012) Mechanisms of Gamma Oscillations. Annu Rev Neurosci 35:203–225

Colgin LL (2016) Rhythms of the hippocampal network. Nat Rev Neurosci 17:239–249

Curti S, Comas V, Rivero C, Borde M (2006) Analysis of behavior-related excitatory inputs to a central pacemaker nucleus in a weakly electric fish. Neuroscience 140:491–504

Dodla R, Wilson CJ (2013) Spike width and frequency alter stability of phase-locking in electrically coupled neurons. Biol Cybern 107:367–383

Dye J (1988) An in vitro physiological preparation of a vertebrate communicatory behavior: chirping in the weakly electric fish, Apteronotus. J Comp Physiol A 163:445–458

Dye J, Heiligenberg W (1987) Intracellular recording in the medullary pacemaker nucleus of the weakly electric fish, Apteronotus, during modulatory behaviors. J Comp Physiol A 161:187–200

Dye J, Heiligenberg W, Keller CH, Kawasaki M (1989) Different classes of glutamate receptors mediate distinct behaviors in a single brainstem nucleus. Proc Natl Acad Sci U S A 86:8993–8997

Elekes K, Szabo T (1985) Synaptology of the medullary command (pacemaker) nucleus of the weakly electric fish (Apteronotus leptorhynchus) with particular reference to comparative aspects. Exp Brain Res 60: 509-520

Ellis DB, Szabo T (1980) Identification of different cell types in the command (pacemaker) nucleus of several gymnotiform species by retrograde transport of horseradish peroxidase. Neuroscience 5:1917–1929

Faber DS, Korn H (1989) Electrical field effects: their relevance in central neural networks. Physiol Rev 69:821–863

Fries P (2009) Neuronal Gamma-Band Synchronization as a Fundamental Process in Cortical Computation. Annu Rev Neurosci 32:209–224

Gonzalez-Burgos G, Cho RY, Lewis DA (2015) Alterations in Cortical Network Oscillations and Parvalbumin Neurons in Schizophrenia. Biol Psychiatry 77:1031–1040

Haider B, McCormick DA (2009) Rapid Neocortical Dynamics: Cellular and Network Mechanisms. Neuron 62:171–189

Hanslmayr S, Staresina BP, Bowman H (2016) Oscillations and Episodic Memory: Addressing the Synchronization/Desynchronization Conundrum. Trends Neurosci 39:16–25

Heiligenberg W, Metzner W, Wong CJH, Keller CH (1996) Motor control of the jamming avoidance response of Apteronotus leptorhynchus: Evolutionary

changes of a behavior and its neuronal substrates. J Comp Physiol - A Sensory, Neural, Behav Physiol 179:653–674

Hupé GJ, Lewis JE (2008) Electrocommunication signals in free swimming brown ghost knifefish, Apteronotus leptorhynchus. J Exp Biol 211:1657–1667

Juranek J, Metzner W (1997) Cellular characterization of synaptic modulations of a neuronal oscillator in electric fish. J Comp Physiol - A Sensory, Neural, Behav Physiol 181:393–414

Juranek J, Metzner W (1998) Segregation of behavior-specific synaptic inputs to a vertebrate neuronal oscillator. J Neurosci 18:9010–9019

Kawasaki M, Heiligenberg W (1988) Individual prepacemaker neurons can modulate the pacemaker cycle of the gymnotiform electric fish, Eigenmannia. J Comp Physiol A 162:13–21

Krahe R, Fortune ES (2013) Electric fishes: neural systems, behaviour and evolution. J Exp Biol 216:2363–2364

Lewis JE (2014) Active electroreception: signals, sensing, and behavior. In: The Physiology of Fishes, Fourth Edition, pp 375–390

Lewis JE, Lindner B, Laliberté B, Groothuis S (2007) Control of neuronal firing by dynamic parallel fiber feedback: implications for electrosensory reafference suppression. J Exp Biol 210:4437–4447

Mancilla JG, Lewis TJ, Pinto DJ, Rinzel J, Connors BW (2007) Synchronization of Electrically Coupled Pairs of Inhibitory Interneurons in Neocortex. J Neurosci 27:2058–2073

Marsat G, Maler L (2010) Neural Heterogeneity and Efficient Population Codes for Communication Signals. J Neurophysiol 104:2543–2555

Moller P (2005) Electric fishes: history and behavior. London: Chapman and Hill

Moortgat KT, Bullock TH, Sejnowski TJ (2000a) Precision of the pacemaker nucleus in a weakly electric fish: network versus cellular influences. J Neurophysiol 83:971–983

Moortgat KT, Bullock TH, Sejnowski TJ (2000b) Gap junction effects on precision and frequency of a model pacemaker network. J Neurophysiol 83:984–997

Moortgat KT, Keller CH, Bullock TH, Sejnowski TJ (1998) Submicrosecond pacemaker precision is behaviorally modulated: the gymnotiform electromotor pathway. PNAS 95:4684–4689

Oestreich J, Zakon HH (2002) The long-term resetting of a brainstem pacemaker nucleus by synaptic input: a model for sensorimotor adaptation. J Neurosci 22:8287–8296

Palmigiano A, Geisel T, Wolf F, Battaglia D (2017) Flexible information routing by transient synchrony. Nat Neurosci 20:1014–1022

Parish G, Hanslmayr S, Bowman H (2018) The Sync/deSync model: How a synchronized hippocampus and a de-synchronized neocortex code memories. J Neurosci:2561–17

Pfeuty B, Mato G, Golomb D, Hansel D (2003) Electrical Synapses and Synchrony: The Role of Intrinsic Currents. J Neurosci 23:6280–6294

Quintana L, Harvey-Girard E, Lescano C, Macadar O, Lorenzo D (2014) Sex-specific role of a glutamate receptor subtype in a pacemaker nucleus controlling electric behavior. J Physiol 108:155–166

Quintana L, Pouso P, Fabbiani G, Macadar O (2011a) A central pacemaker that underlies the production of seasonal and sexually dimorphic social signals: anatomical and electrophysiological aspects. J Comp Physiol A 197:75–88

Quintana L, Sierra F, Silva A, Macadar O (2011b) A central pacemaker that underlies the production of seasonal and sexually dimorphic social signals: functional aspects revealed by glutamate stimulation. J Comp Physiol A 197:211–225

Salazar VL, Krahe R, Lewis JE (2013) The energetics of electric organ discharge generation in gymnotiform weakly electric fish. J Exp Biol 216:2459–2468

Smith AR, Proffitt MR, Ho WW, Mullaney CB, Maldonado-Ocampo JA, Lovejoy NR, Alves-Gomes JA, Smith GT (2016) Evolution of electric communication signals in the South American ghost knifefishes (Gymnotiformes: Apteronotidae): A

phylogenetic comparative study using a sequence-based phylogeny. J Physiol Paris 110:302–313

Smith G, Zakon H (2000) Pharmacological characterization of ionic currents that regulate the pacemaker rhythm in a weakly electric fish. J Neurobiol 42:270–286

Smith GT, Lu Y, Zakon HH (2000) Parvocells: a novel interneuron type in the pacemaker nucleus of a weakly electric fish. J Comp Neurol 423:427–439

Spellman TJ, Gordon JA (2015) Synchrony in schizophrenia: A window into circuit-level pathophysiology. Curr Opin Neurobiol 30:17–23

Steriade M (2006) Grouping of brain rhythms in corticothalamic systems. Neuroscience 137:1087–1106

Stiefel KM, Gutkin BS, Sejnowski TJ (2008) Cholinergic Neuromodulation Changes Phase Response Curve Shape and Type in Cortical Pyramidal Neurons Ermentrout B, ed. PLoS One 3:e3947

Timofeev I, Steriade M (2004) Neocortical seizures: Initiation, development and cessation. Neuroscience 123:299–336

Turner CR, Derylo M, de Santana CD, Alves-Gomes JA, Smith GT (2007) Phylogenetic comparative analysis of electric communication signals in ghost knifefishes (Gymnotiformes: Apteronotidae). J Exp Biol 210:4104–4122

Vervaeke K, LÖrincz A, Gleeson P, Farinella M, Nusser Z, Silver RA (2010) Rapid Desynchronization of an Electrically Coupled Interneuron Network with Sparse Excitatory Synaptic Input. Neuron 67:435–451

Walz H, Hupé GJ, Benda J, Lewis JE (2013) The neuroethology of electrocommunication: How signal background influences sensory encoding and behaviour in Apteronotus leptorhynchus. J Physiol 107:13–25

Wang X-J (2010) Neurophysiological and Computational Principles of Cortical Rhythms in Cognition. Physiol Rev 90:1195–1268

Warrington J (2008) Chirping in vitro: Cellular mechanisms of electrocommunication signal generation in the pacemaker nucleus of Apteronotus leptorhynchus. MSc

Thesis, University of Ottawa

Zakon H, Oestreich J, Tallarovic S, Triefenbach F (2002) EOD modulations of brown ghost electric fish: JARs, chirps, rises, and dips. J Physiol Paris 96:451–458

Zupanc GKH (2017) Dynamic neuron-glia interactions in an oscillatory network controlling behavioral plasticity in the weakly electric fish, Apteronotus leptorhynchus. Front Physiol 8:1–7

Zupanc GKH, Sîrbulescu RF, Nichols A, Ilies I (2006) Electric interactions through chirping behavior in the weakly electric fish, Apteronotus leptorhynchus. J Comp Physiol A 192:159–173

Figure legends

Figure 1. The pacemaker nucleus (Pn) and the electric organ discharge (EOD).
(A) Lower: outline of fish showing schematic relationship between the medullary Pn network (gray outline) and the electric organ (gray line). Upper: schematic network diagram showing electrically-coupled pacemaker (P) and relay (R) neurons; the Pn receives synaptic inputs from the prepacemaker nucleus (PPn), while relay axons project down the spinal cord to set the timing of the EOD.
(B) Recording of the quasi-sinusoidal EOD showing the amplitude modulation (orange) during an electrocommunication signal called a *chirp*; vertical scale bar is 10mV and time scale is shown in panel C.
(C) Instantaneous frequency (1/period) for each cycle of the EOD waveform in panel B shows a change from 1000Hz to 1030Hz during the chirp; vertical scale, 30Hz, and time scale, 10ms.

Figure 2. Example recordings of membrane potential from pairs of neurons in the pacemaker nucleus (Pn).
(A) Paired intracellular recordings from a pacemaker (P) and relay (R) neuron during electrical stimulation of the PPn inputs (indicated by stim arrow) in an *in vitro* Pn preparation. Convention for quantifying responses to stimulation are shown above: control cycle period and three post-stimulus cycle periods are denoted T0, T1, T2, T3 respectively. Time scale bar is 5ms and vertical scale bar is 20mV (applies to both panels A and B).
(B) Intracellular recordings from a single P neuron for two different trials (indicated by black and gray lines) with electrical stimulation of the PPn inputs (indicated by stim arrow) at the same phase (indicated by the arrow) but producing different responses (compare first post-stimulus cycle: 2.4ms and 2.0ms). For display purposes, the stimulus artefact was filtered locally, but in these recordings a downward deflection that differed between trials remained, giving the impression of different stimulus timing when in fact the timing was the same.

Figure 3. Phase resetting curves for neurons in the pacemaker nucleus (Pn).
(A) Resetting curve shows post-stimulus cycle durations (T1, T2, T3) normalized by the control duration T0 as a function of stimulus phase θ for both P (open blue) and R (open red) neurons (29 P cells and 11 R cells in 8 *in vitro* Pn preparations).
(B) T1 responses in panel A shown at higher magnification. In addition, example responses from two individual neurons are shown with filled symbols (P in blue, R in red).

Figure 4. Stimulus-induced changes in neuron phase relationships.
(A) Illustration showing action potentials from two neurons along with the definition for the phase difference, ϕ (i.e. the time Δt between spikes relative to the control period T0).
(B) Stacked histogram of phase differences (absolute value) between the neuron pairs in our sample, color-coded by pair type: PP, pacemaker-pacemaker; PR, pacemaker-relay; RR, relay-relay.
(C) Change in phase difference ($\Delta\phi$) between pairs of neurons for the same stimuli shown in Fig. 3, plotted against post-stimulus cycle number (20 pairs in 8 preparations). Colored symbols show all data for each pair type; boxplots are for data combined across pair type: middle line is median, box hinges denote the 1st and 3rd quartiles, and whiskers are 1.5 times the interquartile range from the hinge point.

Figure 5. Responses of model Pn networks to synaptic input.
Example traces from three different networks of model pacemaker (P) and relay (R) neurons. (A) and (B) show responses of Network 1 to two different stimulus phases (stimulus 1 and 2), while (C) and (D) show the responses of Networks 2 and 3 to stimulus 1. In all panels, membrane potentials for all R and P neurons are overlaid and shown in red and blue respectively (upper), so the thickness of the traces is related to the level of synchrony; the stimulus trace is shown in dark gray (lower): g_{syn} = 90nS was delivered simultaneously to 15 relay cells (stimulated cells in dark red). Time and voltage scales are 2ms and 40mV, shown in panel D.

Figure 6. Phase resetting in a model Pn network.

(A) and (B) show phase resetting curves, as in Fig. 3, for model R and P neurons in one network; responses for all neurons of each type are combined to show the variation across the network, with individual responses indicated by the points and black lines indicating the means. Stimulus: g_{syn} = 90nS applied to 10 R neurons.

(C) and (D) show mean values for T1 and T2 on a magnified scale for R and P neurons respectively and three different stimulus magnitudes (see legend and text for full description). The dashed line in the lower panels indicates the median of T2 for the experimental data in Fig. 3 for the corresponding cell type; median for T1 for the data was 1.0 and 0.99 for R and P neurons respectively and is not shown in the figure.

Figure 7. Stimulus-induced changes in phase difference for model networks.

(A) Change in phase difference ($\Delta\phi$) between pairs of model neurons for each pair type (see legend); boxplots are for responses combined across pair type as in Fig. 4C. Stimulus as in Fig. 6A,B.

(B) Variability in the change in phase difference for different stimulus magnitudes, as quantified by 1.5 times the interquartile range from the 1st and 3rd quartiles (i.e. range spanned by the whiskers of the boxplot in panel A). Experimental data is indicated by the black open circles.

Figure 8. The influence of model network connectivity on chirp properties.

Panels show changes in three different stimulus-response properties as a function of interconnectivity of P neurons (P:P) for both P (blue) and R (red) for gap junctional conduction of 5nS (left panels) and 15nS (right panels). Response properties are: (A and B) "chirp FM", indicated by the minimum cycle duration in the first 5 post-stimulus cycles (averaged over all cells); (C and D) "chirp AM", indicated by the maximum variation in $\Delta\phi$ between cell pairs (peaks in Fig. 7B); and (E and F) "chirp duration", as indicated by the number of cycles required for neurons to re-synchronize following a stimulus (indicated by a median $\Delta\phi$ within ±0.01). Stimulus magnitude: 90nS input to 15 R cells.

Figure 9. The influence of model network connectivity on network stability

Percent of randomized model networks (100 total) that recover to the synchronous state within 10 post-stimulus cycles, at different levels of P:P connectivity and g_c=5ns, 10nS and 15nS (see legend). Stimulus magnitude: 90nS input to 15 R cells.

Table 1. Model parameters for pacemaker and relay neurons

	Pacemaker		**Relay**	
	soma	**axon**	**soma**	**axon**
d_s (cm)	0.030	--	0.065	--
d_a (cm)	--	0.008	--	0.007
l_a (cm)	--	0.045	--	0.040
g_a (mS)	0.0045	0.0045	0.00075	0.00075
$C^{\dagger}$ (μF)	$1.0A_s$	$1.0A_c$	$1.0A_s$	$1.0A_c$
g_L (mS)	$0.3A_s$	$1.0A_c$	$1.0A_s$	$1.0A_c$
g_{Na} (mS)	$500A_s$	$500A_c$	$500A_s$	$500A_c$
g_K (mS)	$20A_s$	$20A_c$	$50A_s$	$50A_c$
I_{bias} (μA)	0.0015	0	0	0
E_{Na} (mV)	50	50	50	50
E_K (mV)	-77.5	-77.5	-77.5	-77.5
E_L (mV)	-70	-70	-70	-70
E_{syn} (mV)	0	0	0	0

$\dagger$ where A_s is surface area of the somatic compartment, and A_c is the surface area of the axonal compartment. Units as shown in first column unless otherwise noted.

Figure 1

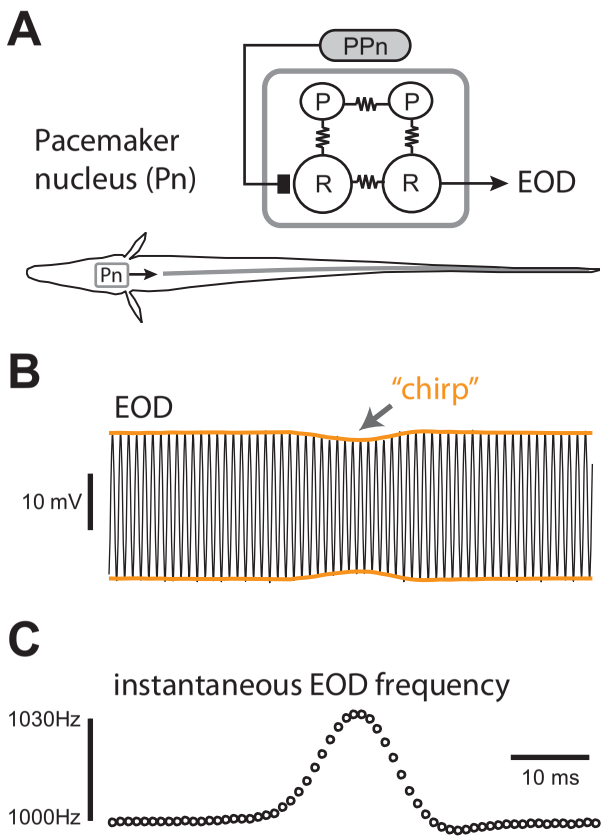
A
PPn
P
P
Pacemaker
nucleus (Pn)
R
R
EOD
Pn
B
EOD
"chirp"
10 mV
C
instantaneous EOD frequency
1030Hz
1000Hz
10 ms

Figure 2

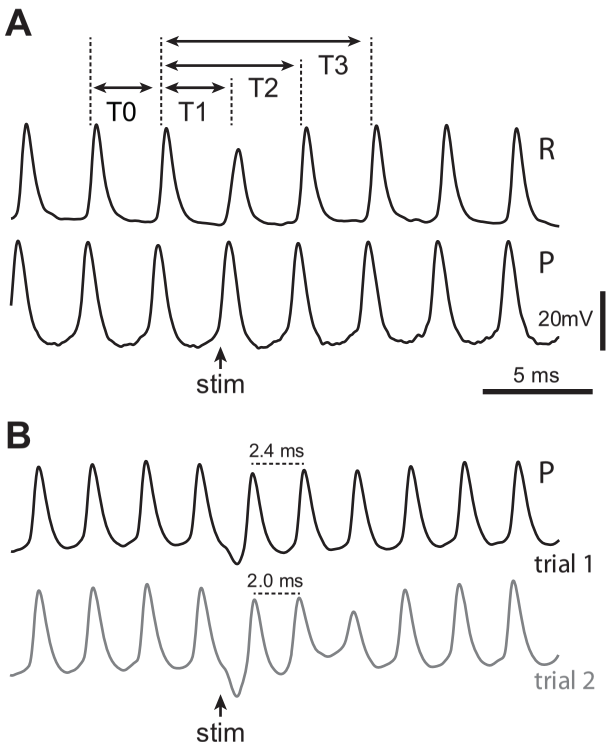

Figure 3

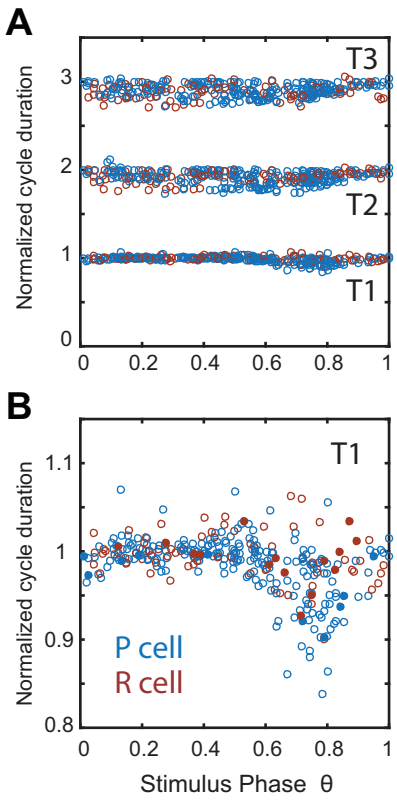
A
T3
T2
T1
Normalized cycle duration
3
2
1
0
0
0.2
0.4
0.6
0.8
1
B
T1
Normalized cycle duration
1.1
1
0.9
0.8
P cell
R cell
0
0.2
0.4
0.6
0.8
1
Stimulus Phase θ

Figure 4

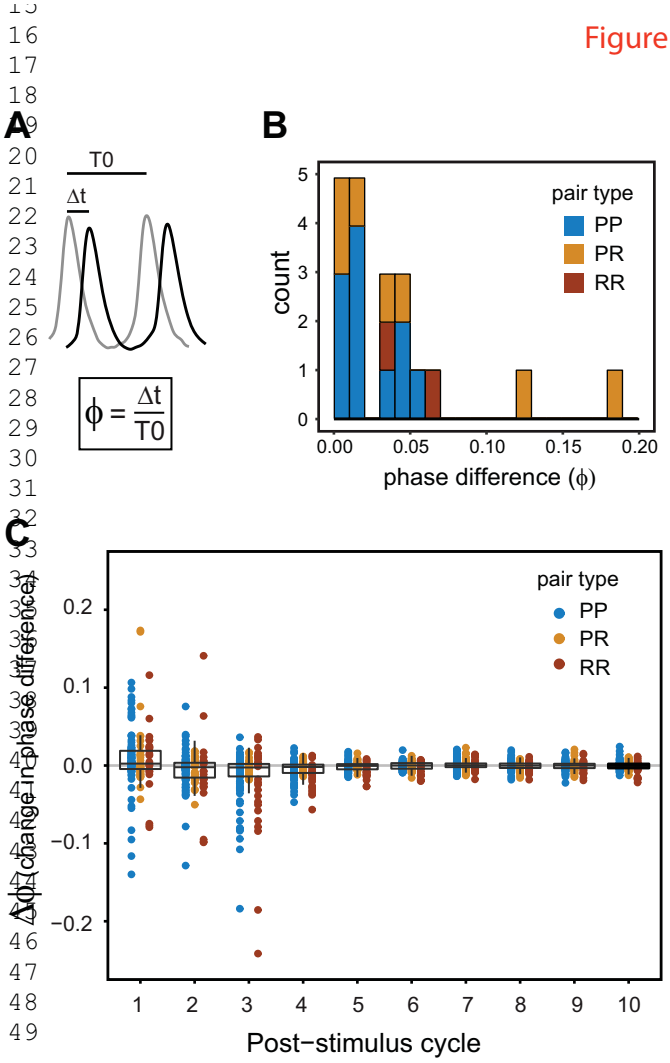
A
T0
Δt
ϕ = Δt / T0
B
pair type
PP
PR
RR
count
phase difference (ϕ)
C
pair type
PP
PR
RR
Δϕ (change in phase difference)
Post−stimulus cycle

Figure 5

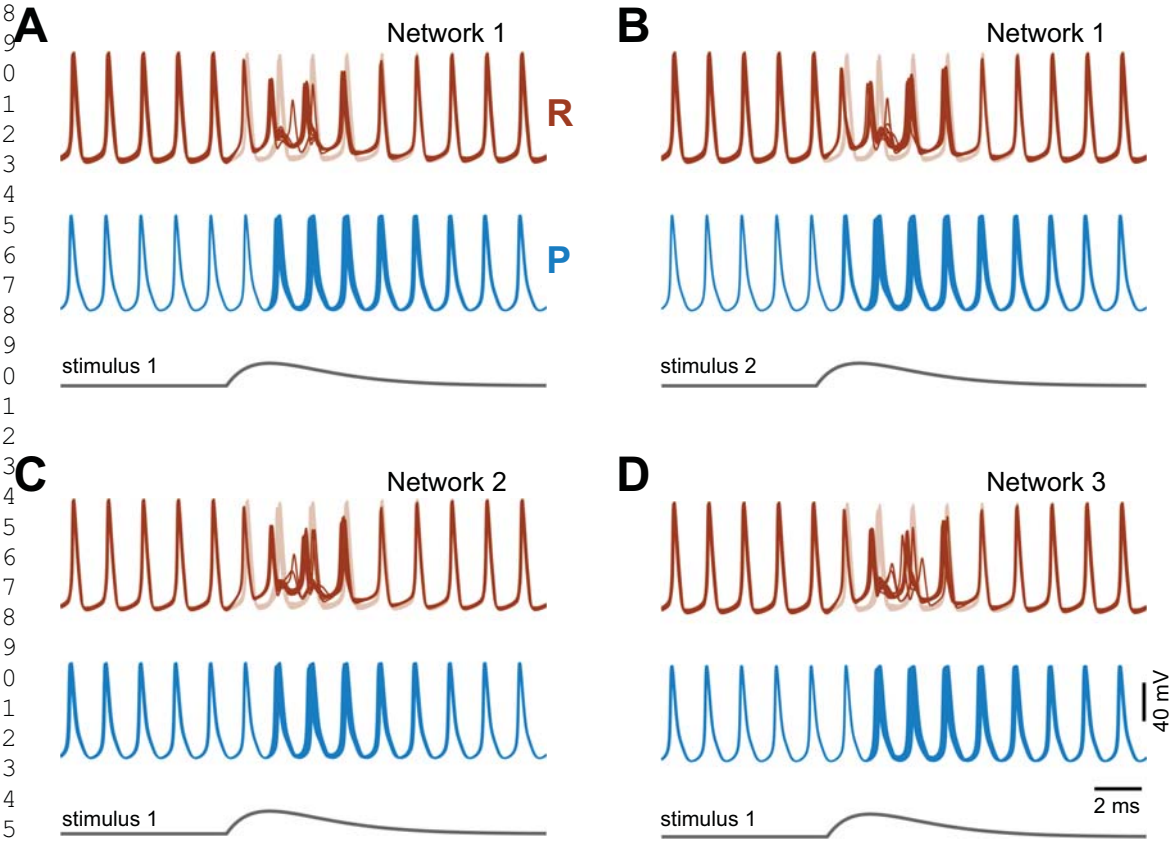
A
Network 1
R
P
stimulus 1
B
Network 1
stimulus 2
C
Network 2
stimulus 1
D
Network 3
40 mV
2 ms
stimulus 1

Figure 6

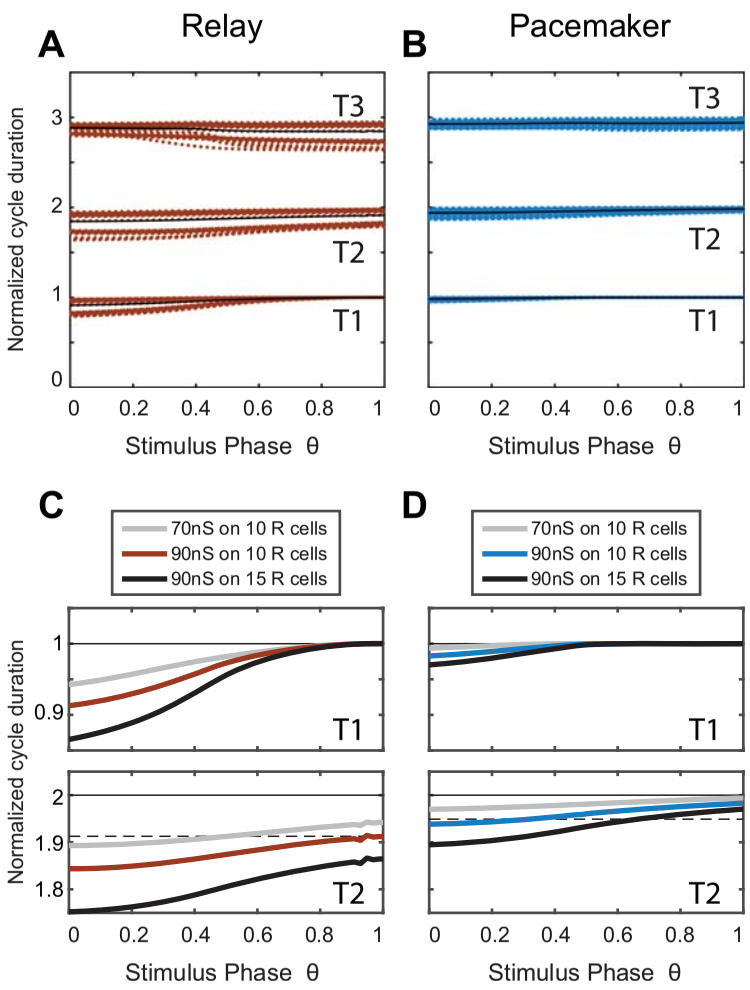
A
Relay
B
Pacemaker
T3
T2
T1
Normalized cycle duration
Stimulus Phase θ
C
D
70nS on 10 R cells
90nS on 10 R cells
90nS on 15 R cells

Figure 7

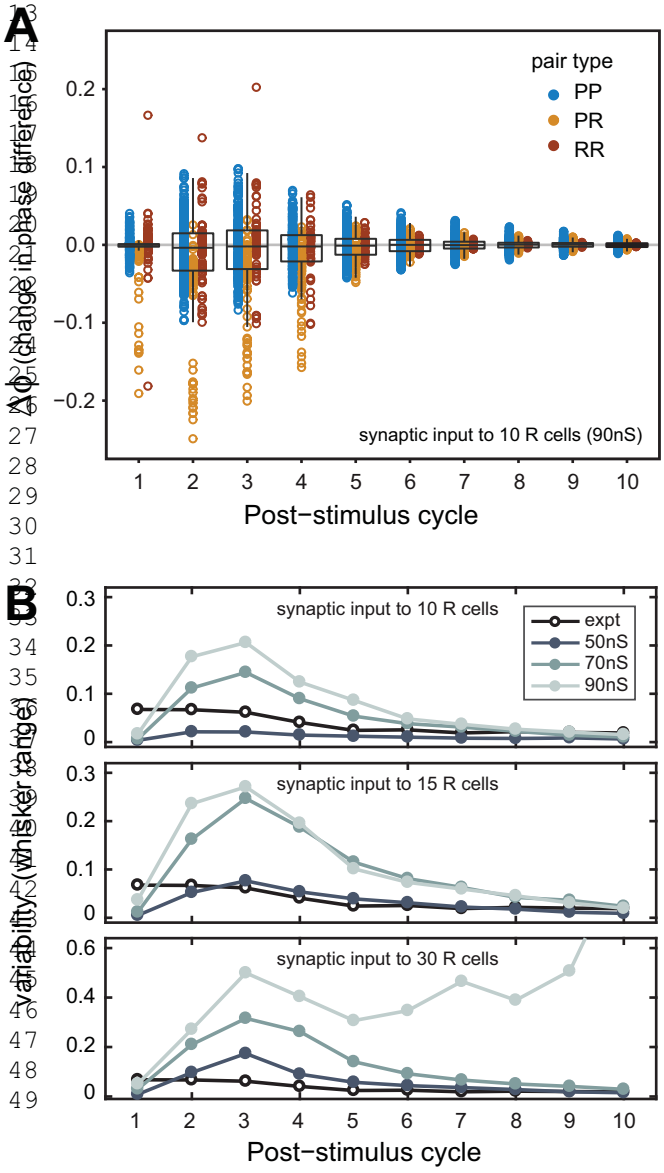
A
pair type
PP
PR
RR
synaptic input to 10 R cells (90nS)
Post−stimulus cycle
B
synaptic input to 10 R cells
expt
50nS
70nS
90nS
synaptic input to 15 R cells
synaptic input to 30 R cells
Post−stimulus cycle

Figure 8

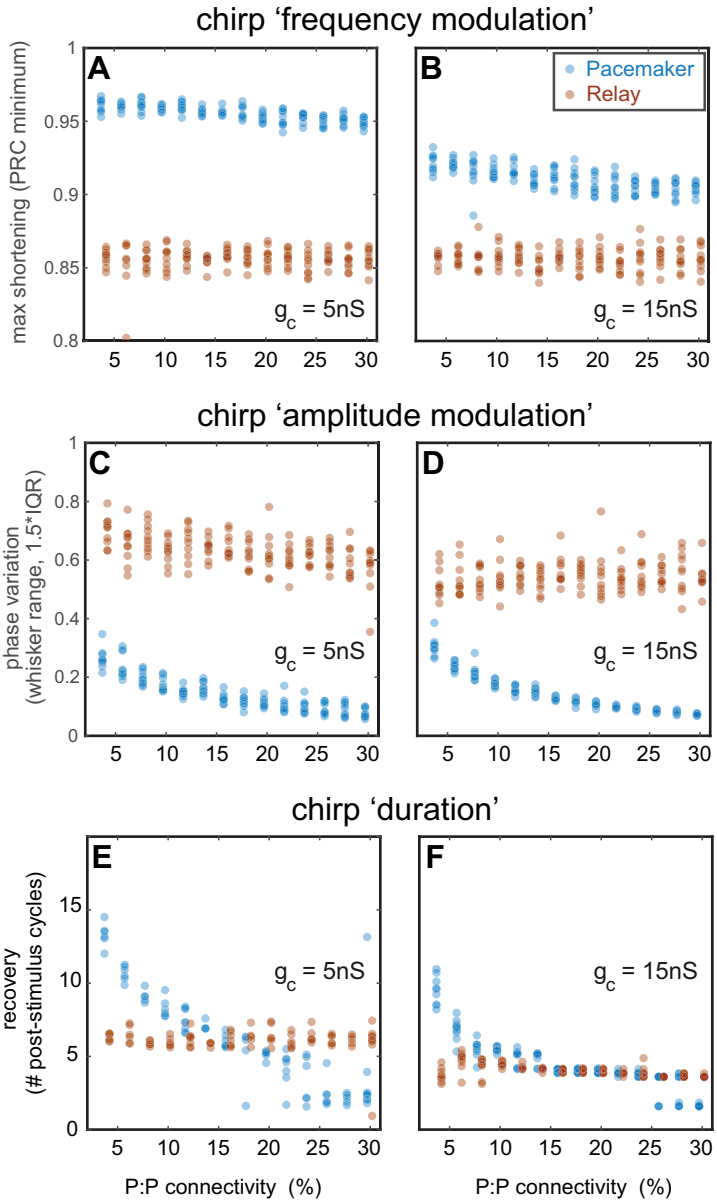
chirp 'frequency modulation'
A
B
Pacemaker
Relay
max shortening (PRC minimum)
1
0.95
0.9
0.85
0.8
g_c = 5nS
g_c = 15nS
5 10 15 20 25 30
chirp 'amplitude modulation'
C
D
phase variation
(whisker range, 1.5*IQR)
1
0.8
0.6
0.4
0.2
0
g_c = 5nS
g_c = 15nS
5 10 15 20 25 30
chirp 'duration'
E
F
recovery
(# post-stimulus cycles)
15
10
5
0
g_c = 5nS
g_c = 15nS
5 10 15 20 25 30
P:P connectivity (%)
P:P connectivity (%)

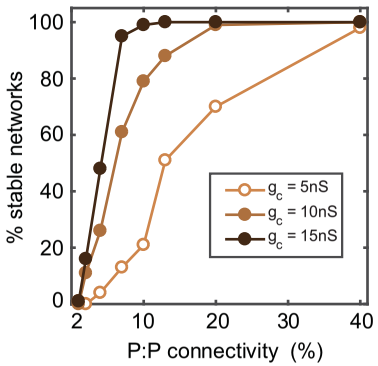
100
80
60
40
20
0
% stable networks
2
10
20
30
40
P:P connectivity (%)
g_c = 5nS
g_c = 10nS
g_c = 15nS

Figure 9